Noble metal-coated probes sliding at up to 100 mm s^{-1} against PZT films for AFM probe-based ferroelectric recording technology

2008 J. Phys.: Condens. Matter 20 225013

(http://iopscience.iop.org/0953-8984/20/22/225013)

IOP Publishing Journal of Physics: Condensed Matter

J. Phys.: Condens. Matter **20** (2008) 225013 (12pp) doi:10.1088/0953-8984/20/22/225013

Noble metal-coated probes sliding at up to 100 mm s^{-1} against PZT films for AFM probe-based ferroelectric recording technology

Bharat Bhushan[1] **and Kwang Joo Kwak**

Nanotribology Laboratory for Information Storage and MEMS/NEMS, The Ohio State University, 201 W. 19th Avenue, Columbus, OH 43210, USA

E-mail: bhushan.2@osu.edu

Received 11 January 2008, in final form 24 February 2008
Published 15 May 2008
Online at stacks.iop.org/JPhysCM/20/225013

Abstract

With the advent of scanning probe microscopes, probe-based data recording technologies are being developed for ultra-high areal density. In the ferroelectric data storage being explored, a conductive atomic force microscope (AFM) tip is scanned over a lead zirconate titanate (PZT) film, which is a ferroelectric material. Ferroelectric domains can be polarized by applying short voltage pulses between the AFM tip and the bottom electrode layer that exceed the coercive field of the PZT film, resulting in nonvolatile changes in the electronic properties. A crucial reliability concern is the wear of the AFM tip and PZT film. The understanding and improvement of tip wear, particularly at the high velocities needed for high-data-rate recording, is critical to the commercialization of ferroelectric data storage. To this end, wear experiments are performed using various noble metal-coated tips sliding against a PZT film at velocities of 10 and 100 mm s^{-1}. The noble metals that were used were Pt, Au–Ni, Pt–Ir and Pt–Ni. High sliding velocities are achieved by using a custom calibrated piezo stage in a commercial AFM. The Au–Ni and Pt–Ir tips are shown to exhibit the lowest wear. The tip wear mechanism is found to be primarily adhesive and abrasive wear, with some evidence of impact wear. The coefficient of friction increases during wear. This study advances the understanding of the physics of friction and wear of noble metal-coated AFM probes.

(Some figures in this article are in colour only in the electronic version)

1. Introduction

Nonvolatile digital data storage systems include electrically addressed systems such as flash memories and mechanically addressed systems such as magnetic tapes, optical disks, and magnetic hard disks (Bhushan 1996, Fazio 2004). The latter has much higher storage capacity and relies on the physical movement of the recording medium or a reading head. Recently, both flash memories and miniature disk drives have begun to replace each other, mostly in portable devices but also in some fixed devices which require a relatively low storage capacity (Coughlin and Handy 2006). Both magnetic hard disks and flash memories show significant technical advances in storage capacity as well as performance and reliability with time. With magnetic recording, most devices use longitudinal recording, where the magnetization prefers to lie in the plane of the recording medium. Perpendicular recording, which has begun to be used, typically exhibits higher limiting areal densities than longitudinal: for example, these densities are projected to be 500 and 100 Gb in^{-2} at a signal-to-noise ratio (SNR) of 20 dB, respectively (Bertram and Williams 2000, Richter 2007). Heat-assisted magnetic recording (HAMR) and recording on bit-patterned media have been identified as future technologies for extending magnetic recording. HAMR recording makes the recording device more complicated. The head structure needs to be augmented by a laser with near-

[1] Author to whom any correspondence should be addressed.

field optical system to accomplish the heating (Rottmayer *et al* 2006). For the bit-patterned media, the media need to have nanopatterns. It is to be noted that the head-medium spacing is one of the important factors for the drastic increase in areal density as well (Bhushan 1996).

With the advent of scanning probe microscopes (SPM), probe-based recording technologies are being developed for ultra-high areal density. Many approaches using probe-based techniques have been brought forward (Cooper *et al* 1999, Shin *et al* 2000, Bhushan 2007). Various recording techniques using thermomechanical (Mamin and Rugar 1992, Vettiger *et al* 1999), phase change (Kado and Tohda 1995, Gidon *et al* 2004, Wright *et al* 2006), magnetic (Ohkubo *et al* 1991), thermomagnetic (Nakamura *et al* 1995, Zhang *et al* 2002), optical (Betzig *et al* 1992), electrical (Barrett and Quate 1991) and ferroelectric (Franke *et al* 1994, Ahn *et al* 1997) methods have been demonstrated. A probe-based storage device with an atomic force microscope (AFM) tip has the potential to achieve ultra-high areal densities on the order of several Tb in^{-2} or higher. Another great advantage of a probe-based recording technique is the use of a multiple probe array for high data rates. IBM group has developed a technology which uses an array of 1024 silicon cantilevers (Millipede) for thermomechanical recording and playback on a polymer which is about 40 nm thick with a harder Si substrate (Vettiger *et al* 1999). The cantilevers consist of integrated heaters with tips of nanoscale dimensions. The tip, heated to about 400 °C, is brought into contact with the polymer for recording. Reading is done using the heated cantilever, originally used for recording, as a thermal readback sensor by exploiting its temperature-dependent resistance. Wear of the heated tip is an issue.

A second technique using a probe-based recording system is phase change memory (PCM) (Kado and Tohda 1995, Gidon *et al* 2004, Wright *et al* 2006), which has the potential for dramatic progress in memory devices (Maimon *et al* 2001, Strand 2005). The pioneering work of Stanford Ovshinsky in the 1960s on switching (Ovshinsky 1968) and memory effects in chalcogenide alloys motivated the field of amorphous semiconductors. Chips based on ovonic unified memory (OUM^{TM}) storage generate different levels of high and low resistance on a glassy material, which represent 1 and 0 states in binary recording. An OUM nonvolatile memory cell uses a horizontal strip of chalcogenide—a type of electrically conductive glass material—connected to an electrode. When a high current is applied through the electrode probe, the chalcogenide medium is heated to more than 630 °C, creating a region of amorphous glass with high resistance. When a lower current is applied, it heats up to a temperature less than 630 °C and then cools to a crystalline state with lower resistance. In the reading mode, a low-level current is passed through the tip to the medium to sense the high-resistance amorphous state or the low-resistance crystalline state. The probe needs to be electrically conductive, and a high-conductivity platinum (Pt) coating can be deposited on the silicon probe. For a fast data transfer rate, the cantilever array needs to be moved at high velocities, on the order of 100 mm s^{-1}. Friction and wear at high velocities, high loads, and in high-temperature conditions are major impediments to this technology (Bhushan and Kwak 2007a). A significant concern is the durability of the probe tips during the recording process at high temperatures during sliding contact at relatively high velocities on the order of tens of mm s^{-1}.

A third technique is ferroelectric memory, which is used as ferroelectric random access memory (FeRAM) in an electrically addressed storage system (Setter *et al* 2006). In FeRAM, the dielectric structure includes ferroelectric material, typically lead zirconate titanate (PZT). When an external electric field is applied across the ferroelectric medium, positive or negative charges will be displaced from their original position—a concept that is characterized by polarization. In a ferroelectric material, there is a spontaneous polarization—a displacement that is inherent to the crystal structure of the material. The direction of this polarization can be reversed or reoriented by applying an electric field. Thus, the application of an electric field can be used to change the polarization direction of the medium; typically, binary 1 and 0 states are stored as one of two possible electric polarizations in each data storage cell.

There are a number of alternative approaches on the basis of ferroelectric materials for nonvolatile data storage such as ferroelectric field-effect transistors (Arimoto and Ishiwara 2004), ferroelectric resistive-based data storage (Blom *et al* 1994) and ferroelectric tunnel junctions (Zhuravlev *et al* 2005). An alternative ferroelectric data storage is a mechanically addressed storage system which uses a probe-based recording technique (Franke *et al* 1994, Hidaka *et al* 1996, Ahn *et al* 1997, Shin *et al* 2002). The schematic of domain writing and reading in ferroelectric films is shown in figure 1. For example, a conductive AFM tip is placed in contact with a storage medium consisting of $SrTiO_3$ (STO), coated with a $PbZr_{0.52}Ti_{0.48}O_3/SrRuO_3$ (PZT/SRO) double layer (Franke *et al* 1994, Ahn *et al* 1997). The SRO serves as the bottom electrode, and PZT represents the ferroelectric film. Ferroelectric domains can be polarized by applying short voltage pulses ($\sim$10 V, $\sim$100 μs) between the AFM tip and the SRO electrode that exceed the coercive field of the PZT layer, resulting in local, nonvolatile changes in the electronic properties of the underlying film. In epitaxial *c*-axis oriented PZT films, the polarization vector can be parallel or antiparallel to the *c*-axis. An example for a series of ferroelectric bits on the domain radius versus pulse duration width has been achieved by Tybell *et al* (2002). The activation energy increases significantly from 50 to 130 MV m^{-1} as the film thickness is reduced from 81 to 29 nm. In principle, thinner PZT films should result in smaller domains and higher storage densities. It should be noted that the temperature rise during recording should be on the order of 80 °C, which alleviates wear issues. Furthermore, the tip does not need to be in contact with the medium during readback.

There are two different methods for reading out the polarization state in a ferroelectric thin film. Imaging of ferroelectric domains in a thin film makes use of the basic properties of ferroelectrics, namely their piezoelectric behavior and the presence of surface charge. A static surface charge, proportional to the normal component of polarization, can

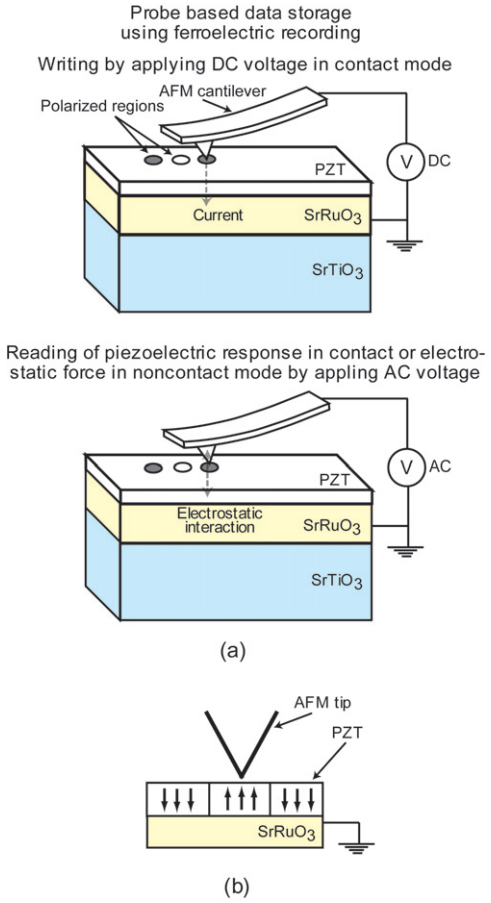

Figure 1. Schematics of the AFM probe-based storage system using ferroelectric media.

be detected by electrostatic force microscopy (EFM), when the microscope is operating in the noncontact mode; see figure 1 (Saurenbach and Terris 1990). A similar detection mechanism has been demonstrated for previously written ferroelectric domains on a PZT/Nb-doped $SrTiO_3$ by Ahn *et al* (1997). In the noncontact regime, these voltage modulation techniques, such as Kelvin probe force microscopy (KPFM), are sensitive to the voltage derivation of the force (Martin *et al* 1988, Nonnenmacher *et al* 1991). In the second method, an AFM is operated in contact mode and the piezoresponse force is measured by applying an ac voltage; the method is called piezoresponse force microscopy (PFM) (Guthner and Dransfeld 1992, Franke *et al* 1994, Gruverman *et al* 1996, Roelofs *et al* 2000). By monitoring the piezoelectric vibration of the ferroelectric film caused by an external ac voltage, the domain structure can be visualized in the AFM piezoresponse mode when the probing tip is in contact with the film surface (Gruverman *et al* 1996). In this piezoresponse mode, the voltage is applied through the probe tip, which is used as a movable top electrode. The modulated deflection signal from the cantilever, which oscillates together with the thin film due to tip–sample contact, is detected using the lock-in amplifier, as in the case of the noncontact detection.

Considering the fidelity of AFM probe-based data storage, it is noted that the application of a voltage pulse to the PZT film results in a change in its thickness. A degradation phenomenon to be considered in connection with the reliability problem is ferroelectric fatigue, or the decrease of switchable polarization with repeated polarization reversal (Mihara *et al* 1994). The understanding and improvement of this polarization fatigue might be the key to the commercialization of high-density ferroelectric memories. Another important reliability issue to be considered in probe-based data storage is tip wear with tip–sample contact (Bhushan and Kwak 2007a). Under typical PFM operating conditions, the total force acting on a tip, F, is equal to $F_0 + F_{el}$, where F_0 ($=kd_0$) is an elastic force exerted by a cantilever of a spring constant k at a set-point deflection, d_0, and F_{el} is an electrostatic force (Kalinin and Bonnell 2002). When a normal force is much larger than the electrostatic force, $F_{el} \ll F_0$, the average stress below a tip is 1.3 GPa for a contact radius of ∼5 nm, corresponding to a normal force of ∼100 nN and a tip radius of 50 nm.

In order to achieve high wear resistance and long lifetime, a high surface hardness of a noble metal-coated tip is essential. However, a noble metal-deposited tip surface has a lower hardness than that of typically used Si tips. The selection of a top metal layer on the tip depends on the material hardness, electrical conductivity, melting point, and deposition processing difficulty. The failure mechanism is particularly severe for soft metals such as pure Au. An alloy such as Au–Ni_5 (gold with an alloying addition of 5% nickel), a hard contact material used in relays, can be used in the selection of the top metal layer. A wear-resistant tip including an alloy of platinum, iridium and tungsten has been introduced for spark plugs by AlliedSignal Inc. (Kozlov *et al* 2000). By adding a small amount of tungsten to platinum–iridium alloy, the wear resistance of the spark plug is improved. Several metals that could potentially provide some of the desirable properties are listed in table 1. It is noted that the metal properties can vary significantly on the basis of the deposition condition of the material. It is well known that the resistivity of a sputtered metal film can be much more than its bulk resistivity (Rooney *et al* 1990, Conoci *et al* 2006). The tip wear mechanism is not well understood on the nanoscale, especially with various top metal layers on the probe tip. Possible wear mechanisms of AFM tip–sample contacts include adhesive wear, abrasive wear, low cycle fatigue, tribochemical wear, and thermally activated stick–slip (Bloo *et al* 1999, Skarman and Wallenberg 2000, Maw *et al* 2002, Su *et al* 2003, Tao and Bhushan 2006a, 2006b, Bhushan and Kwak 2007a, 2007b). A single or multiple mechanisms can be responsible for tip wear, depending on the operating conditions.

In this work, a comprehensive investigation of friction and wear of tips coated with various noble metals sliding against a PZT film is performed at a range of loads and sliding distances. A silicon grating sample and software to deconvolute the tip shape are used to characterize the change in the tip shape and evaluate the tip radius and its wear volume.

2. Experimental details

2.1. Experimental samples

The probes used in this study were etched single-crystal silicon probes coated with Pt, Au–Ni, Pt–Ir and Pt–Ni films. For Pt

Table 1. Details of noble metal-coated probes.

	Tip		
Noble metal	Stiffness (N m^{-1}) and initial 2D tip radius (nm)	Thickness of metal films (nm)	PZT flat sample
Pt (baseline)	∼2 N m^{-1}, 74 nm (CSC21, MikroMasch)	185 nm/15 nm Pt/Cr (sputter deposition)	−15 nm/50 nm $PbZr_{0.2}Ti_{0.8}O_3/SrRuO_3$ film on 0.5 mm *c*-axis $SrTiO_3$ (pulse laser deposition)
Au–Ni	∼2.8 N m^{-1}, 65 nm Au–Ni (FM) (PPP-FM, Nanosensors)	65 nm/10 nm Au–Ni/Cr (sputter deposition with Au–Ni alloy, and sputtering with Cr target, respectively)	
	∼0.2 N m^{-1}, 38 nm Au–Ni (CT) (PPP-CONT, Nanosensors)	33 nm/10 nm Au–Ni/Cr (sputter deposition with Au–Ni alloy target)	
Pt–Ir	∼2.8 N m^{-1}, 53 nm Pt–Ir (FM) (PPP-EFM, Nanosensors)	25 nm/3 nm Pt–Ir/Cr (sputter deposition)	
Pt–Ni	∼2.8 N m^{-1}, 61 nm Pt–Ni (FM) (PPP-FM, Nanosensors)	95 nm/10 nm Pt–Ni/Ni (co-sputtering with separate Pt and Ni targets, and sputtering with Ni target, respectively)	
	∼0.2 N m^{-1}, 48 nm Pt–Ni (CT) (PPP-CONT, Nanosensors)	33 nm/10 nm Pt–Ni/Ni (co-sputtering with separate Pt and Ni targets, and sputtering with Ni target, respectively)	

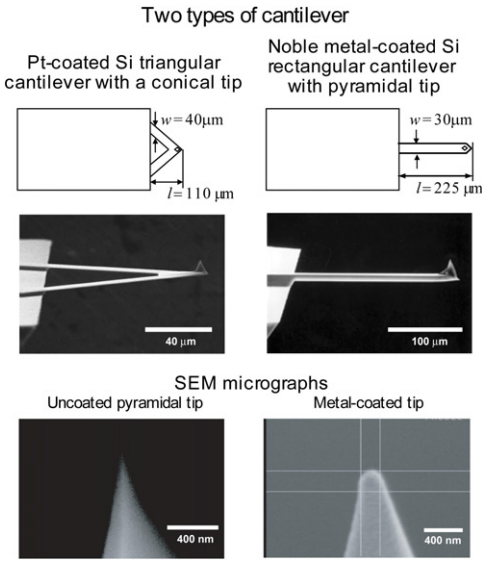

Figure 2. Schematics and photographs of (a) a triangular V-shaped and (b) a rectangular cantilever with metal-coated layer.

probes, triangular silicon cantilevers with conical probe tips (CSC21, MikroMasch) were coated with 185 nm/15 nm thick Pt/Cr using sputter deposition (figure 2). The length and width of both cantilever legs were 110 and 40 μm, respectively. The nominal spring constant of the cantilever and tip radius are 2 N m^{-1} and 10 nm before coating (provided by the manufacturer), respectively. The coatings are expected to lead to a slight increase in the spring constant and tip radius. For Au–Ni (FM) and Pt–Ni (FM) probes, rectangular silicon cantilevers with pyramidal probe tips (PPP-FM, Nanosensors) were coated. Au–Ni (FM) probes were coated with a 65 nm/10 nm thick Au–Ni/Cr bilayer using sputter deposition with an Au–Ni alloy target and a Cr target, respectively. Pt–Ni (FM) probes were coated with a 95 nm/10 nm thick Pt–Ni/Ni bilayer using co-sputtering deposition with separate Pt and Ni targets and sputtering with a Ni target, respectively. The length and width of the cantilevers were 225 and 30 μm, respectively. For Pt–Ir (FM) probes, rectangular silicon cantilevers with pyramidal probe tips (PPP-EFM, Nanosensors) were coated with 25 nm/3 nm thick Pt–Ir/Cr. The nominal spring constant of the cantilever was 2.8 N m^{-1} for all three, and the tip radius was 10 nm before coating with Au–Ni or Pt–Ni and 25 nm for Pt–Ir (provided by the manufacturer). To study the stiffness effect, compliant rectangular silicon cantilevers with pyramidal probe tips were used with the nominal spring constant of the cantilever and a tip radius of 0.2 N m^{-1} and 10 nm (PPP-CONT, Nanosensors), respectively. The bilayer Au–Ni/Cr (33 nm/10 nm thick) and Pt–Ni/Ni (33 nm/10 nm thick) coatings were applied for Au–Ni (CT) and Pt–Ni (CT) probes, respectively. The probes details used in this study are summarized in table 1.

The initial two-dimensional (2D) tip radius is an important factor in the wear rate. The initial radius also depends on the thickness of the coated-metal films. The deposition condition of the metal films, such as the deposition angle and deposition rate, affects the initial shape and 2D radius. The tip radius and probe shape strongly affect the contact area between the tip and the PZT film during the wear experiments. The larger contact area tends to increase wear volume in sliding on the PZT film. After the coating is removed, the Si tip substrate is exposed, and then the wear volume increases rapidly with an increase in the sliding distance. The initial tip radii for various tips are also listed in table 1.

For the PZT disk sample, the PZT film was deposited on a 50 nm thick $SrRuO_3$ (SRO) film grown by pulse laser

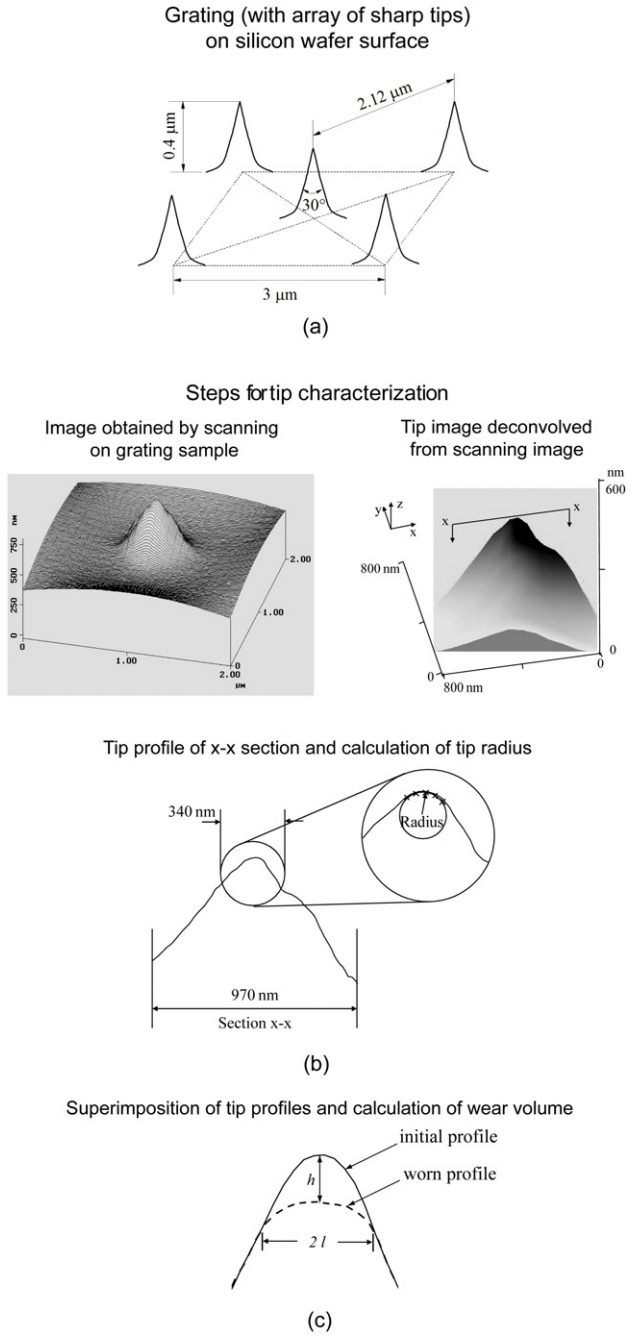

Figure 3. (a) Schematic of a grating (with an array of sharp tips) on a silicon wafer surface, (b) illustration of tip characterization and calculation of tip radius, and (c) illustration of calculation of the wear volume.

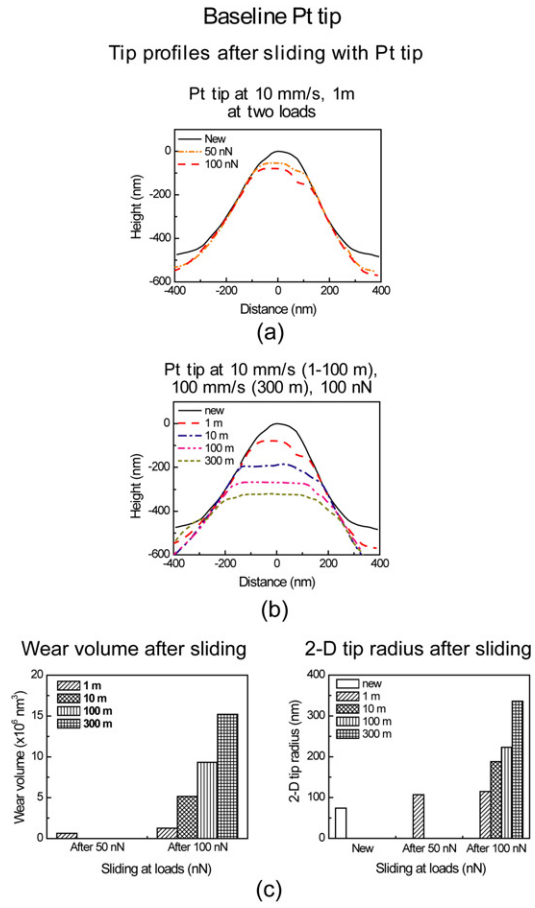

Figure 4. (a) Pt tip profiles before and after 1 m sliding, 10 mm s^{-1} and at 50 nN, after additional 1 m sliding at 100 nN on a PZT film; (b) tip profiles before and after 1, 10 and 100 m sliding at 10 mm s^{-1}, and 300 m sliding at 100 mm s^{-1} and at 100 nN on the same film. The solid curve corresponds to the virgin tip profile, and (c) wear volumes and 2D tip radii after 1 m at 50 nN and 1, 10, 100 m sliding at 10 mm s^{-1}, and 300 m sliding at 100 mm s^{-1}.

deposition (PLD) on a 0.5 mm thick *c*-axis $SrTiO_3$ (STO) substrate. PLD was also used to deposit the 15 nm thick PZT film with a Zr/Ti composition ratio of 20/80 ($PbZr_{0.2}Ti_{0.8}O_3$). The surface morphology was observed using an AFM with a $10 \times 10\ \mu m^2$ scan, and the root mean square (RMS) roughness of the PZT film was about 2 nm.

2.2. Tip shape characterization

A silicon TGT1 grating sample (NT-MDT, Moscow, Russia) was used for probe tip characterization (Tao and Bhushan 2006a, 2006b, Bhushan and Kwak 2007a, 2007b). The grating sample has an array of sharp tips on the surface (see figure 3(a)). The tips are arranged on each corner and at the center of a $3 \times 3\ \mu m^2$ square area. The height of each tip is 0.4 μm. The tip angle is about 30°, and the radius of the tip is less than 10 nm. SPIP™ software (Scanning Probe Image Processor, Image Metrology A/S, Denmark) was used to characterize the tip and evaluate the tip radius. The processing procedure is illustrated in figure 3(b). The image was first obtained in tapping mode by scanning the tip on the TGT1 grating sample in a direction perpendicular to the long axis of cantilever beam. Scanning was performed on a $2 \times 2\ \mu m^2$ scan area with a velocity of 1 μm s^{-1}. The three-dimensional (3D) surface of the tip was generated with 970 nm × 970 nm size (63 points × 63 points) using a blind tip reconstruction algorithm from the scanned image (Villarrubia 1994). Even if the probe tip has an asymmetric shape, a simple semicircle could be more easily fitted on the 2D tip profile than a hemisphere to a 3D surface; therefore, the 2D tip radius was calculated. The algorithm was used to generate a 2D profile from the tip surface in the scanning direction at the highest location. The tip radius

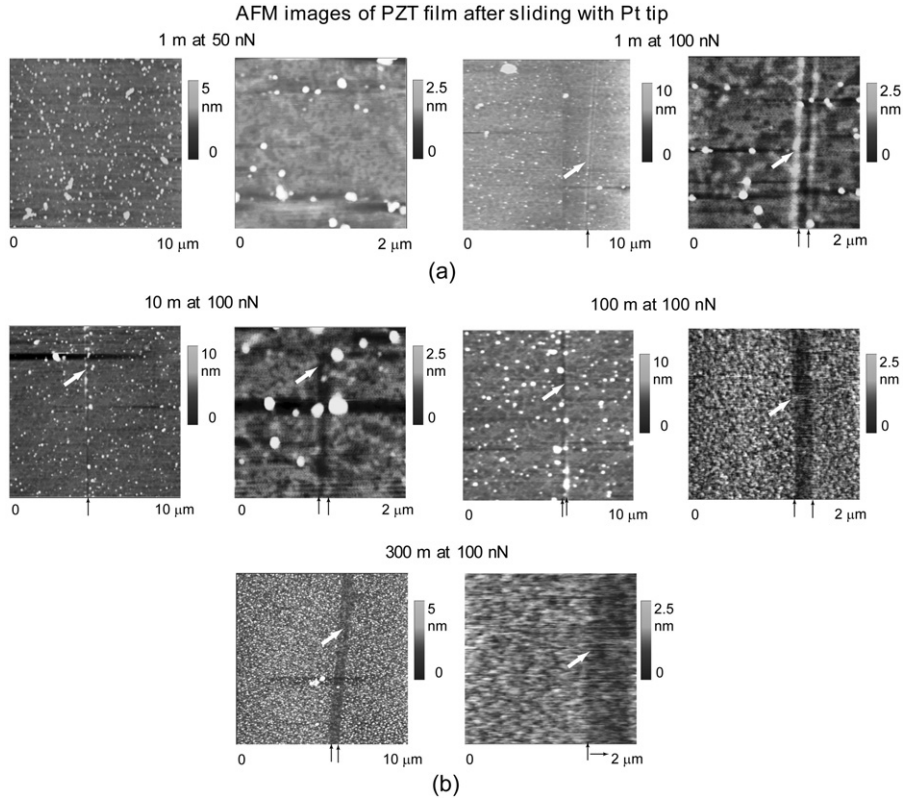

Figure 5. (a) AFM images obtained after 1 m of sliding with a Pt tip, 10 mm s^{-1} and at 50 nN, after additional 1 m of sliding at 100 nN on a PZT film, and (b) AFM images obtained after 10 and 100 m of sliding at 10 mm s^{-1}, and 300 m of sliding at 100 mm s^{-1} and at 100 nN on the same film. If a wear scar can be detected, black arrows are used to identify them and white arrows indicate significant damage.

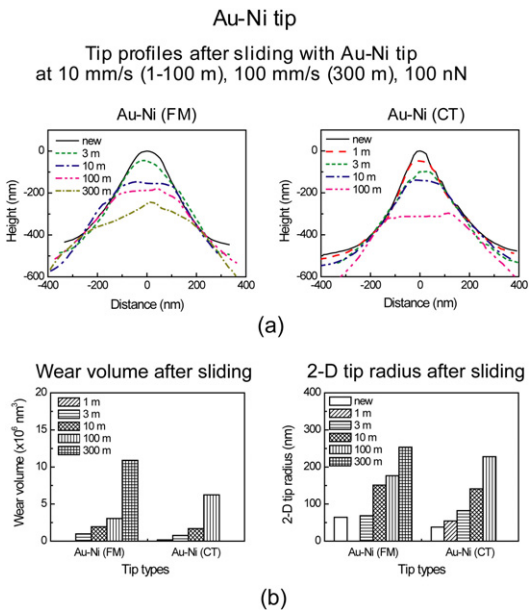

Figure 6. (a) Au–Ni tip profiles before and after 1, 3, 10, 30 and 100 m of sliding at 10 mm s^{-1}, and 300 m of sliding at 100 mm s^{-1} and at 100 nN on the PZT film, and (b) wear volumes and 2D tip radii after 1, 3, 10, 30 and 100 m of sliding at 10 mm s^{-1}, and 300 m of sliding at 100 mm s^{-1} and at 100 nN on the same film.

was calculated for a profile with several tens of nanometers in length by a circle fitted with at least five data points (15.4 nm apart) using the SPIP software.

2.3. Friction force and wear measurement

Friction and wear tests were conducted using a Dimension 3000 AFM (Digital Instruments). Measurements were performed in an ambient environment (22 ± 1 °C, 50 ± 5% relative humidity), unless specified. The friction force experiments were carried out by scanning the sample along an axis perpendicular to the long axis of the cantilever, at a scan velocity of 1 μm s^{-1} using a scan rate of 0.5 Hz at normal loads ranging from 1 to 80 nN. The effect of z-piezo movement on the normal load due to thermal drift was monitored and was found to be within 10%. The measured friction force was plotted as a function of the normal load. The data could be fitted with a straight line, which suggests that the friction force is proportional to the normal load. The coefficient of friction was obtained by calculating the slope of the line (Ruan and Bhushan 1994, Bhushan 2002, 2005).

For wear experiments, a high-velocity piezo stage, developed by Tao and Bhushan (2006c), was used at sliding velocities of 10 mm s^{-1} (frequency = 10 Hz) and 100 mm s^{-1} (frequency = 50 Hz). The system includes a custom calibrated piezo stage or a piezo ultrasonic linear drive (M663.465, Physik Instrumente, GmbH & Co. KG, Karlsruhe, Germany), a stage controller (C865, Physik Instrumente), and a self-designed software application for operation control. A sliding velocity of 10 mm s^{-1} was used for a maximum sliding distance of 100 m. A higher velocity at 100 mm s^{-1} was used for a total sliding distance of 300 m to reduce the test duration. The length of a single line scan for the line profile

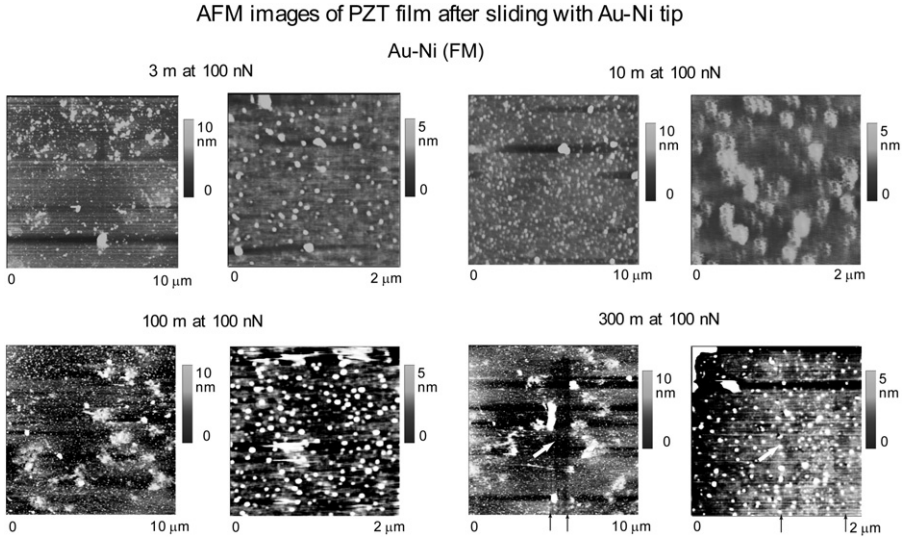

Figure 7. AFM images obtained after 3, 10 and 100 m of sliding with Au–Ni (FM) tip at 10 mm s^{-1} and 100 nN, an additional 300 m of sliding at 100 mm s^{-1} and at 100 nN on the PZT film. If wear scar can be detected, black arrows are used to identify them and white arrows indicate significant damage.

mode was 500 and 1000 μm for average sliding velocities of 10 and 100 mm s^{-1}, respectively. For sliding distances of 1, 3, 10, 30 and 100 m, the sliding duration was 1×10^2, 3×10^2, 1×10^3, 3×10^3 and 1×10^4 s, respectively, at a sliding velocity of 10 mm s^{-1}. For the remaining 200 m distance, the sliding duration was 2×10^3 s at a sliding velocity of 100 mm s^{-1}. The scan direction was parallel to the long axis of the cantilever beam.

In order to determine the maximum normal load that can be used for the wear experiments with wear measurable with the SPIP technique employed here, first the baseline experiments were performed using a Pt tip at loads of 50 and 100 nN. The wear experiments were run at 50 nN for a 1 m sliding distance, followed by tests at a load of 100 nN for a 1 m sliding distance at 10 mm s^{-1} (Bhushan and Kwak 2007a). Based on the baseline experiments, it was found that a normal load of 100 nN can be used with measurable wear, and this was selected. Subsequent tests were conducted at a 100 nN load for a sliding distance of the first 100 m at 10 mm s^{-1} and of the remaining 200 m at 100 mm s^{-1}.

For wear measurements, each probe was first scanned on the grating sample in tapping mode to obtain the initial image for tip characterization (Tao and Bhushan 2006a, Bhushan and Kwak 2007a). After scanning on the grating sample, the tip was slid on a PZT film sample in contact mode. After the wear test, the probe was scanned again on the grating sample to obtain an image for tip characterization. The wear volume was calculated from the tip profiles before and after the wear experiment. In order to calculate the wear volume, the profile after sliding was manually superimposed with the original profile so that they coincide (largely) with each other; see figure 3(c). The worn region was assumed to be cone-shaped. The worn height (h) of the cone was the distance between the tops of the original and the worn tips, and the $2l$ was the width of the base of the worn region. The wear volume was calculated as $V = \pi l^2 h/3$.

To further understand the wear mechanisms, the worn tips were imaged using a field emission scanning electron microscope (FE-SEM; Hitachi S-4300) operating at 10 kV and 5 μA under 1.2×10^{-7} Pa. The virgin tips were examined for reference as well to check the uniformity of the top metal coating.

3. Results and discussion

3.1. Wear and friction experiments with various tips

Figure 4(a) shows Pt tip profiles before and after 1 m of sliding at 10 mm s^{-1} and 50 nN, and after an additional 1 m of sliding at 10 mm s^{-1} and 100 nN on a PZT film. The reduction in height indicates tip blunting resulting from wear, and this is seen in all cases. Figure 5(a) shows the surface height images obtained after wear experiments. A wear scar was not observed after 1 m of sliding at 50 nN on the PZT film. The sliding cycles (round trips) were only 1000 cycles during 1 m sliding, and it is not surprising that no wear scar exists under the low normal load of 50 nN. A wear scar was observed after an additional 1 m of sliding at 100 nN on the PZT film. From these baseline experiments, it was found that a normal load of 100 nN can be used with measurable wear, and this was selected for further experiments.

Figure 4(b) shows Pt tip profiles taken after sliding for 1, 10, 100 and 300 m for a Pt-coated tip at 100 nN. The data for wear volumes and tip radii are summarized in figure 4(c). For comparison with data to be presented later, the wear volume and 2D tip radius were obtained as about 9.3×10^6 nm^3 and 223 nm, respectively, after 100 m of sliding. Figure 5(b) shows the surface height images obtained after 10, 100, and 300 m of sliding on the same film. At these sliding distances, wear scars were observed on the PZT film. A wear depth of PZT is observed to be about 1 nm after 10 m sliding at 100 nN. At sliding distances of 100 and 300 m, wear occurs over a larger

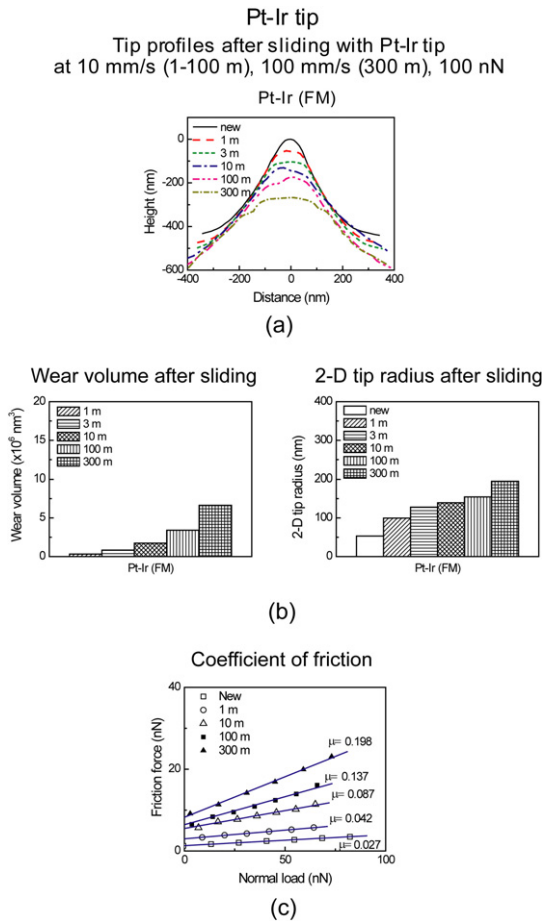

Figure 8. (a) Pt–Ir tip profiles before and after 1, 3, 10, 30 and 100 m of sliding at 10 mm s^{-1}, and 300 m of sliding at 100 mm s^{-1} and at 100 nN on the PZT film, (b) wear volumes and 2D tip radii after 1, 3, 10, 30 and 100 m of sliding at 10 mm s^{-1}, and 300 m of sliding at 100 mm s^{-1} and at 100 nN on the same film, and (c) friction force as a function of the normal load, obtained by measuring friction forces with a Pt–Ir (FM) tip at increasing normal loads in the range of 1–80 nN after 1, 10, 100 and 300 m of sliding on the PZT film.

area due to blunting of the tip as well as the thermal drift after sliding for some time.

Figure 6(a) shows the tip profiles taken after sliding for 3, 10, 100 and 300 m for Au–Ni (FM) tips. The Au–Ni-coated tips used for sliding against the PZT film did not wear as fast as the Pt-coated tips. It should be noted that the data for tip profiles are not available for the Au–Ni-coated tip after 300 m of sliding at 100 nN because the tip had worn beyond the characterization limit of the SPIP software. Figure 6(b) summarizes the wear volume and 2D tip radius as a function of the sliding distance. The wear volume and 2D tip radius for Au–Ni (FM) tips were calculated to be about 3.1×10^6 nm^3 and 176 nm, respectively, after 100 m of sliding at 100 nN. Data for the wear volume and 2D tip radius that are presented closely track each other in figure 6(b). Figure 7 shows the surface height images obtained after 3, 10, 100 and 300 m of sliding on the same film. At a 300 m sliding distance, wear scars were observed on the PZT film. If a wear scar can be detected, black arrows are used to identify them, and white arrows indicate significant damage. A wear depth of PZT is observed to be about 1.5 nm after 300 m of sliding. However, at a sliding distance of 100 m or lower, wear scars could not be identified on the PZT film. At a sliding distance of 300 m, wear occurs over a larger area due to blunting of the tip as well as the thermal drift after sliding for some time.

Figure 8(a) shows the Pt–Ir (FM) tip profiles taken after sliding for 1, 3, 10, 100 and 300 m. Figure 8(b) summarizes the wear volume and 2D tip radius as a function of the sliding distance. The wear volume and 2D tip radius for Pt–Ir (FM) samples were calculated to be about 3.4×10^6 nm^3 and 115 nm, respectively, after 100 m sliding at 100 nN. Data for the wear volume and 2D tip radius that are shown in figure 8(b) closely track each other. Figure 9 shows the surface height images obtained after 3, 10 and 100 m of sliding on the PZT film.

In order to investigate the friction properties between the probe tips and the PZT film, the friction force as a function of the normal load was measured, as shown in figure 8(c). For a virgin Pt–Ir (FM) tip, the coefficient of friction (μ) increases from 0.027 to 0.042 after 1 m of sliding at 100 nN. The increase in the tip radius after sliding leads to a larger contact area, leading to higher adhesion, which increases the friction force and the measured value of μ. At sliding distances of 10 and 100 m, μ increased from 0.042 to 0.067 and 0.137 at 100 nN, respectively. The μ increased from 0.137 to 0.198 after 300 m of sliding.

Figure 10(a) shows the Pt–Ni (FM) tip profiles taken after sliding for 1, 3, 10 and 100 m. Data for a sliding distance of 300 m are not reported because the wear was excessive, and the worn tip profile could not be analyzed. Figure 10(b) summarizes the wear volume and 2D tip radius as a function of sliding distance. The wear volume and 2D tip radius for Pt–Ni (FM) samples were calculated to be about 7.2×10^6 nm^3 and 257 nm, respectively, after 100 m sliding at 100 nN. Figure 11 shows the surface height images obtained after 1, 3, 10 and 100 m of sliding on the PZT film. At a 100 m sliding distance, wear scars were observed on the PZT film image of 10×10 μm^2 scan area. However, at a sliding distance of 10 m or lower, wear scars could not be observed on any PZT film images. At a sliding distance of 100 m, wear occurs over a larger area due to blunting of the tip as well as the thermal drift after sliding for some time.

In addition to characterizing the probe tip, the tip shapes after sliding were examined by an SEM. Figure 12 shows SEM images of virgin Pt, Au–Ni, Pt–Ir and Pt–Ni tips compared to worn tips after 300 m, 300 m, 300 m, and 100 m of sliding on the PZT film, respectively. Significant wear is observed in all cases after sliding. The wear of Pt-coated tip is higher than for other metal-coated tips, as noted earlier. The Pt–Ir tip is shown to exhibit less wear compared to the Au–Ni tip. In particular, the exposed under-layer of the Si part is clearly shown in the Au–Ni tip after 300 m of sliding. Further analysis of the worn tip surface using a spectroscopic method can be considered for chemical elucidation.

3.2. Cantilever stiffness effect

In order to study the cantilever stiffness effect, Au–Ni (CT) and Pt–Ni (CT) coated tips with compliant levers were tested. In the case of a cantilever with a small spring constant of

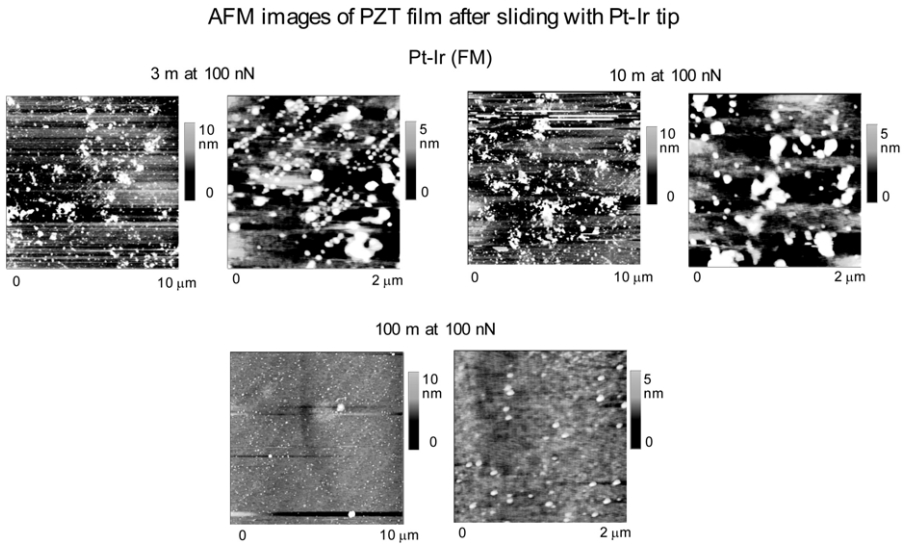

Figure 9. AFM images obtained after 3, 10, 30 and 100 m of sliding with a Pt–Ir (FM) tip at 10 mm s^{-1} and at 100 nN on the PZT film.

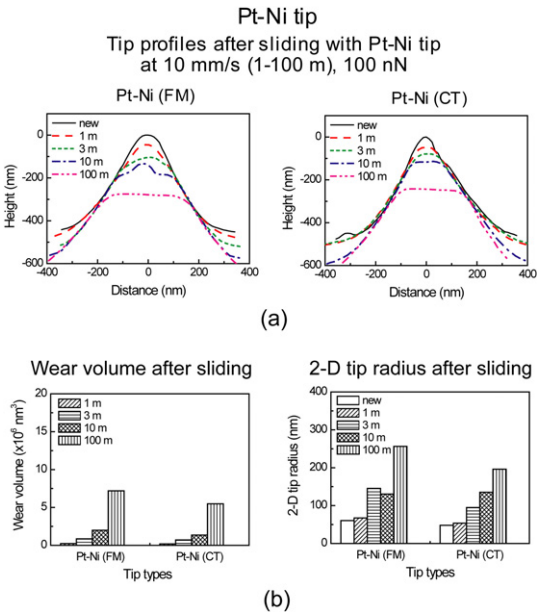

Figure 10. (a) Pt–Ni tip profiles before and after 1, 3, 10, 30 and 100 m of sliding at 10 mm s^{-1} and at 100 nN on the PZT film, and (b) wear volumes and 2D tip radii after 1, 3, 10, 30 and 100 m of sliding at 10 mm s^{-1} and at 100 nN on the same film.

0.2 N m^{-1}, tip characterization is conducted using contact-mode AFM, because the tip was unstable in the tapping mode. The tip profiles after sliding of Au–Ni (FM) and Au–Ni (CT) tips are shown in figure 6(a). The wear for Au–Ni (FM) is lower than that for Au–Ni (CT) in figure 6(b). We believe that the stiffer cantilever dampens any vibrations at high sliding velocity. The tip profiles and wear volume and 2D tip radius data for Pt–Ni (FM) and Pt–Ni (CT) are presented in figures 10(a) and (b), respectively. The wear obtained using stiff and compliant cantilevers is comparable.

3.3. Discussion of wear mechanisms

The wear volume and 2D tip radius as a function of sliding distance are summarized in figure 13 for all tips. The data at 100 m with stiff cantilevers are summarized in table 2. The Pt-coated tip, which consists of a Pt/Cr coating on Si, experienced considerable wear, as shown in the tip profiles. The Pt-coated tip surface is significantly softer than the PZT film surface. The PZT film as the ferroelectric medium has a surface hardness of about 13 GPa and elastic modulus of about 200 GPa (Fang *et al* 2003, Palacio and Bhushan 2008b). For a Pt-coated tip as a typical conductive metal, the average hardness and elastic modulus values of Pt metal at room temperature are about 0.42 and 171 GPa (Davis 1998), respectively. However, the composite hardness and modulus of the layered tips is higher (Palacio and Bhushan 2008a). The Au–Ni and Pt–Ir tips are shown to exhibit less wear compared to the Pt tips, with Pt–Ni of intermediate values. Alloying of Pt can improve the mechanical properties. Pt–Ni and Pt–Ir coated tips are known to have slightly higher hardness and elastic modulus than a Pt tip (Palacio and Bhushan 2008a). In the scratch experiments performed by Palacio and Bhushan (2008a), it was determined that the primary deformation mode is plastic deformation. The Pt–Ir and Pt coatings showed the highest and lowest scratch resistance, respectively. Scratch results are found to show comparable trends with these wear experiments.

Table 2. Summary of wear volumes and tip radii for various tips after sliding tests for 100 m.

Noble metal	Wear volume ($\times 10^6$ nm^3)	Tip radius (nm)
Pt (baseline)	9.3	233
Au–Ni (FM)	3.1	176
Pt–Ir (FM)	3.4	115
Pt–Ni (FM)	7.2	257

The wear mechanism depends on the tip radius, the tip and sample materials, and the operating conditions. Wear of the tip could be caused by various mechanisms (Bhushan 2002, 2005). AFM images of wear scars and SEM images of worn tips show plowing of PZT material and pile up in the wear tracks, and plastic deformation of the tip, which is indicative of adhesive wear. Tip profiles provide evidence of an irregular

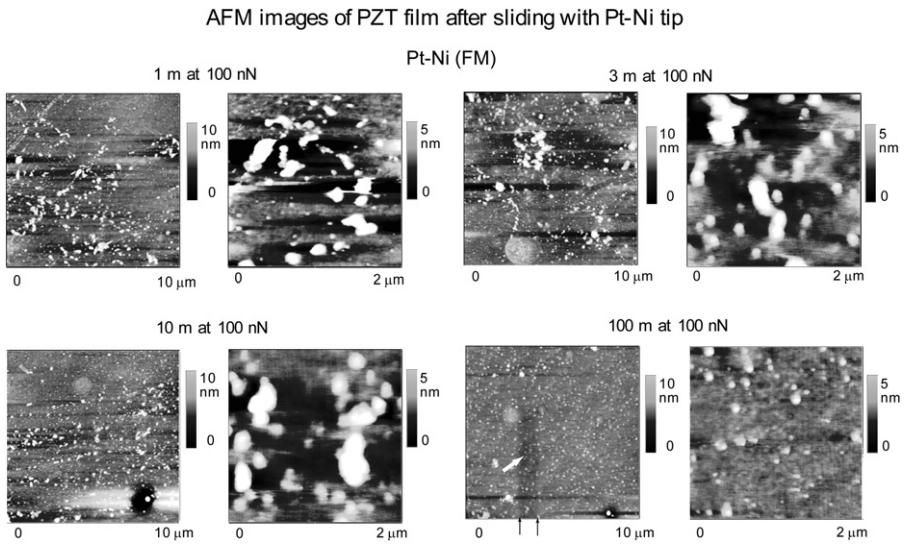

Figure 11. AFM images obtained after 1, 3, 10 and 100 m of sliding with a Pt–Ni (FM) tip at 10 mm s^{-1} and at 100 nN on the PZT film. If a wear scar can be detected, black arrows are used to identify them and white arrows indicate significant damage.

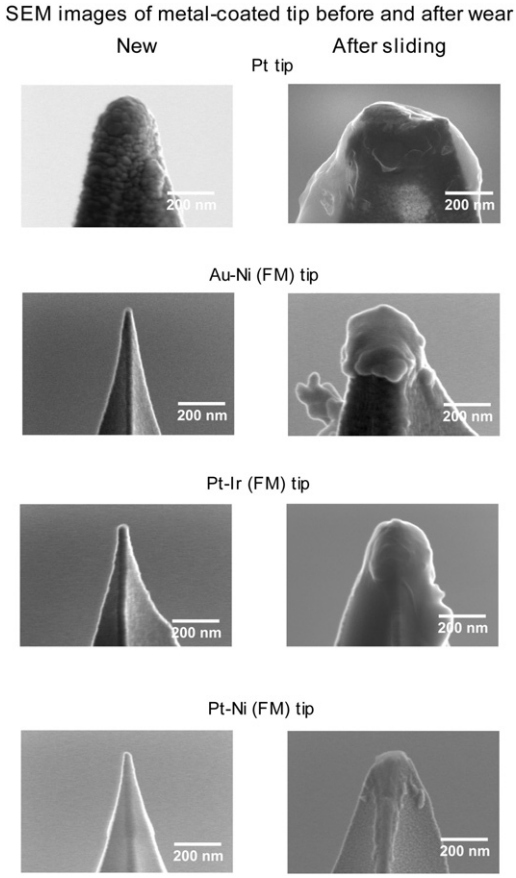

Figure 12. SEM images of the Pt, Au–Ni, Pt–Ir and Pt–Ni tips obtained before and after sliding at 100 nN on the PZT film for 300 m, 300 m, 300 m, and 100 m, respectively.

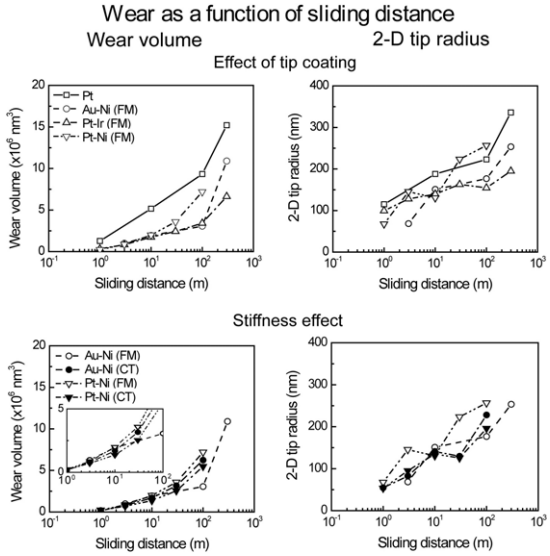

Figure 13. Wear volumes and 2D tip radii were plotted as a function of sliding distance for Pt, Au–Ni, Pt–Ir and Pt–Ni tips. An inset was added in one of the figures to magnify the stiffness effect.

worn surface, indicating abrasive wear, especially after long sliding distances. Brittle platinum-coated silicon asperities can fracture when sliding against the film surface. Particles would be produced by the fracture of asperities. These particles stay between the contacting surfaces and could accelerate the abrasive wear (Bhushan 2002, 2005, Tao and Bhushan 2006a). At high velocities, the impact of asperities becomes important and wear could be caused by periodic high-velocity impact on the PZT film surface (Tambe and Bhushan 2005, Tao and Bhushan 2007, Bhushan and Kwak 2007a, 2007b, Kwak and Bhushan 2008).

4. Conclusions

Wear studies at sliding velocities of 10 and 100 mm s^{-1} were conducted on Pt, Au–Ni, Pt–Ir, and Pt–Ni coated tips sliding on PZT film, a ferroelectric medium for a total sliding distance of 300 m. The Au–Ni and Pt–Ir tips are shown to exhibit less wear

compared to the Pt tips, with Pt–Ni of intermediate values. The tip wear mechanism is primarily adhesive and abrasive wear with some evidence of impact wear. The coefficient of friction increases sliding wear. Based on reported experiments on the effect of the cantilever stiffness on tip wear, stiffness does not appear to play a significant role. This study advances the understanding of the physics of friction and wear of noble metal-coated AFM probes.

References

Ahn C H, Tybell T, Antognazza L, Char Z, Hammond R H, Beasley M R, Fischer O and Triscone J-M 1997 Local, nonvolatile electronic writing of epitaxial $Pb(Zr_{0.52}Ti_{0.48})O_3/SrRuO_3$ heterostructures *Science* **276** 1100–3

Arimoto Y and Ishiwara H 2004 Current status of ferroelectric random-access memory *MRS Bull.* **29** 823–6

Barrett R C and Quate C F 1991 Charge storage in a nitride-oxide-silicon medium by scanning capacitance microscopy *J. Appl. Phys.* **70** 2725–33

Bertram H N and Williams M 2000 SNR and density limit estimates: a comparison of longitudinal and perpendicular recording *IEEE Trans. Magn.* **36** 4–9

Betzig E, Trautman J K, Wolfe R, Gyorgy E M, Finn P L, Kryder M H and Chang C-H 1992 Near-field magneto-optics and high density data storage *Appl. Phys. Lett.* **61** 142–4

Bhushan B 1996 *Tribology and Mechanics of Magnetic Storage Devices* 2nd edn (New York: Springer)

Bhushan B 2002 *Introduction to Tribology* (New York: Wiley)

Bhushan B 2005 *Nanotribology and Nanomechanics—An Introduction* (Heidelberg: Springer)

Bhushan B 2007 *Springer Handbook of Nanotechnology* 2nd edn (Berlin: Springer)

Bhushan B and Kwak K J 2007a Platinum-coated probes sliding up to 100 mm s^{-1} against coated silicon wafers for AFM probe-based recording technology *Nanotechnology* **18** 345504

Bhushan B and Kwak K J 2007b Velocity dependence of nanoscale wear in atomic force microscopy *Appl. Phys. Lett.* **91** 163113

Blom P W M, Wolf R M, Cillessen J F M and krijin M P C M 1994 Ferroelectric schottky diode *Phys. Rev. Lett.* **73** 2107–10

Bloo M L, Haitjema H and Pril W O 1999 Deformation and wear of pyramidal, silicon-nitride AFM tips scanning micrometre-size features in contact mode *Measurement* **25** 203–21

Conoci S, Petralia S, Samorì P, Raymo F M, Bella S D and Sortino S 2006 Optically transparent, ultrathin Pt films as versatile metal substrates for molecular optoelectronics *Adv. Funct. Mater.* **16** 1425–32

Cooper E B, Manalis S R, Fang H, Dai H, Matsumoto K, Minne S C, Hunt T and Quate C F 1999 Tatabit-per-square-inch data storage with the atomic force microscope *Appl. Phys. Lett.* **75** 3566–8

Coughlin T and Handy J 2006 Flash versus hard drives: the battle intensifies *Solid State Tech.* **49** S14–8

Davis J R 1998 *Metals Handbook: Desk Edition* 2nd edn (Materials Park, OH: ASM International)

Fang T-H, Jian S-R and Chuu D-S 2003 Nanomechanical properties of lead zirconate titanate thin film by nanoindentation *J. Phys.: Condens. Matter* **15** 5253–9

Fazio A 2004 Flash memory scaling *MRS Bull.* **29** 814–7

Franke K, Besold J, Haessler W and Seegebarth C 1994 Modification and detection of domains on ferroelectric PZT films by scanning force microscopy *Surf. Sci.* **302** L283–8

Gidon S, Lemonnier O, Rolland B, Bichet O, Dressler C and Samson Y 2004 Electrical probe storage using Joule heating in phase change media *Appl. Phys. Lett.* **85** 6392–4

Gruverman A, Auciello O and Tokumoto H 1996 Scanning force microscopy for the study of domain structure in ferroelectric thin films *J. Vac. Sci. Technol.* B **14** 602–5

Guthner P and Dransfeld K 1992 Local poling of ferroelectric polymers by scanning force microscopy *Appl. Phys. Lett.* **61** 1137–9

Hidaka T, Maruyama T, Saitoh M, Mikoshiba N, Shimizu M, Shiosaki T, Wills L A, Hiskes R, Dicarolis S A and Amano J 1996 Formation and observation of 50 nm polarized domains in $PbZr_{1-x}Ti_xO_3$ thin film using scanning probe microscope *Appl. Phys. Lett.* **68** 2358–9

Kado H and Tohda T 1995 Nanometer-scale recording on chalcogenide films with an atomic force microscope *Appl. Phys. Lett.* **66** 2961–2

Kalinin S V and Bonnell D A 2002 Imaging mechanism of piezoresponse force microscopy of ferroelectric surfaces *Phys. Rev.* B **65** 125408

Kozlov A, Chang C-F, Taylor R D, Franz L R and Leone E A 2000 Wear-resistant spark plug electrode tip containing platinum alloys, spark plug containing the wear-resistant tip, and method of making same *US Patent Specification* 6071163

Kwak K J and Bhushan B 2008 Platinum-coated probes sliding at up to 100 mm s^{-1} against PZT films for AFM probe-based ferroelectric recording technology *J. Vac. Sci. Technol.* A at press

Maimon J, Spall E, Quinn R and Schnur S 2001 Chalcogenide-based non-volatile memory technology *Proc. IEEE Aerosp. Conf.* **5** 2289–94

Mamin H J and Rugar D 1992 Thermomechanical writing with an atomic force microscope tip *Appl. Phys. Lett.* **61** 1003–5

Martin Y, Abraham D W and Wickramasinghe H K 1988 High-resolution capacitance measurement and potentiometry by force microscopy *Appl. Phys. Lett.* **52** 1103–5

Maw W, Stevens F, Langford S C and Dickinson J T 2002 Single asperity tribochemical wear of silicon nitride studied by atomic force microscopy *J. Appl. Phys.* **92** 5103–9

Mihara T, Watanabe H and Araujo C A P 1994 Polarization fatigue characteristics of sol–gel ferroelectric $Pb(Zr_{0.4}Ti_{0.6})O_3$ thin-film capacitors *Japan. J. Appl. Phys.* **33** 3996–4002

Nakamura J, Miyamoto M, Hosaka S and Koyanagi H 1995 High-density thermomagnetic recording method using a scanning tunneling microscope *J. Appl. Phys.* **77** 779–81

Nonnenmacher M, O'Boyle M P and Wickramasinghe H K 1991 Kelvin probe force microscopy *Appl. Phys. Lett.* **58** 2921–3

Ohkubo T, Kishigami J, Yanagisawa K and Kaneko R 1991 Submicron magnetizing and its detection based on the point magnetic recording concept *IEEE Trans. Magn.* **27** 5286–8

Ovshinsky S R 1968 Reversible electrical switching phenomena in disordered structures *Phys. Rev. Lett.* **21** 1450–3

Palacio M and Bhushan B 2008a Nanomechanical and nanotribological characterization of noble metal-coated AFM tips for probe-based ferroelectric data recording *Nanotechnology* **19** 105705

Palacio M and Bhushan B 2008b Nanotribological and nanomechanical properties of lubricated PZT thin films for ferroelectric data storage applications *J. Vac. Sci. Technol.* A at press

Richter H J 2007 The transition from longitudinal to perpendicular recording *J. Phys. D: Appl. Phys.* **40** R149–77

Roelofs A, Bottger U, Waser R, Schlaphof F, Trogisch S and Eng L M 2000 Differentiating 180° and 90° switching of ferroelectric domains with three-dimensional piezoresponse force microscopy *Appl. Phys. Lett.* **77** 3444–6

Rooney D, Negrotti D, Byassee T, Macero D, Chaiken J and Vastag B 1990 Use of laser-directed chemical vapor deposition to fabricate durable, optically transparent, platinum thin film electrode *J. Electrochem. Soc.* **137** 1162–6

Rottmayer R E, Batra S, Buechel D, Challener W A, Hohlfeld J, Kubota Y, Li L, Lu B, Mihalcea C, Mountfield K, Pelhos K, Peng C, Rausch T, Seigler M A, Weller D and Yang X M 2006 Heat-assisted magnetic recording *IEEE Trans. Magn.* **42** 2417–21

Ruan J and Bhushan B 1994 Atomic-scale friction measurements using friction force microscopy: part I—general principles and new measurement techniques *ASME J. Tribol.* **116** 378–88

Saurenbach F and Terris B D 1990 Imaging of ferroelectric domain walls by force microscopy *Appl. Phys. Lett.* **56** 1703–5

Setter N, Damjanovic D, Eng L, Fox G, Gevorgian S, Hong S, Kingon A, Kohlstedt H, Park N Y, Stephenson G B, Stolitchnov I, Taganstev A K, Taylor D V, Yamada T and Streiffer S 2006 Ferroelectric thin films: review of materials, properties, and applications *J. Appl. Phys.* **100** 051606

Shin H, Hong S, Moon J and Jeon J U 2002 Read/write mechanisms and data storage system using atomic force microscopy and MEMS technology *Ultramicroscopy* **91** 103–10

Shin H, Lee K M, Moon W K, Jeon J U, Lim G, Pak Y E, Park J H and Yoon K H 2000 An application of polarized domains in ferroelectric thin films using scanning probe microscope *IEEE Trans. Ultrason. Ferroelectr. Freq. Control* **47** 801–7

Skarman B and Wallenberg L R 2000 Evaluation of intermittent contact mode AFM probes by HREM and using atomically sharp CeO_2 ridges as tip characterizer *Langmuir* **6** 6267–77

Strand D 2005 Ovonics: from science to products *J. Optoelec. Adv. Mater.* **7** 1679–90

Su C, Huang L, Kjoller K and Babcock K 2003 Studies of tip wear processes in tapping mode atomic force microscopy *Ultramicroscopy* **97** 135–44

Tambe N S and Bhushan B 2005 Friction model for the velocity dependence of nanoscale friction *Nanotechnology* **16** 2309–24

Tao Z and Bhushan B 2006a Surface modification of AFM silicon probes for adhesion and wear reduction *Tribol. Lett.* **21** 1–16

Tao Z and Bhushan B 2006b Surface modification of AFM Si_3N_4 probes for adhesion/friction reduction and imaging improvement *ASME J. Tribol.* **128** 865–75

Tao Z and Bhushan B 2006c A new technique for studying nanoscale friction at sliding velocities up to 200 mm s^{-1} using atomic force microscope *Rev. Sci. Instrum.* **77** 103705

Tao Z and Bhushan B 2007 Velocity dependence and rest time effect on nanoscale friction of ultrathin films at high sliding velocities *J. Vac. Sci. Technol.* A **25** 1267–74

Tybell T, Paruch P, Giamarchi T and Triacone J-M 2002 Domain wall creep in epitaxial ferroelectric $Pb(Zr_{0.2}Ti_{0.8})O_3$ thin films *Phys. Rev. Lett.* **89** 097601

Vettiger P, Brugger J, Despont M, Drechsler U, Durig U, Haberle W, Lutwyche M, Rothuizen H, Stutz R, Widmer R and Binnig G 1999 Ultrahigh density, high-data-rate NEMS-based AFM data storage system *J. Microelectron. Eng.* **46** 11–7

Villarrubia J S 1994 Morphological estimation of tip geometry for scanned probe microscopy *Surf. Sci.* **321** 287–300

Wright C D, Armand M and Aziz M M 2006 Terabit-per-square-inch data storage using phase-chang media and scanning electrical nanoprobes *IEEE Trans. Nanotechnol.* **5** 50–61

Zhang L, Bain J A and Zhu J-G 2002 Dependence of thermal-magnetic mark size on applied STM voltage in Co/Pt multilayers *IEEE Trans. Magn.* **38** 1895–7

Zhuravlev M Y, Sabirianov R F, Jaswal S S and Tsymbal E Y 2005 Giant electroresistance in ferroelectric tunnel junctions *Phys. Rev. Lett.* **94** 246802